Subcycle engineering of laser filamentation in gas by harmonic seeding

P. Béjot,* G. Karras, F. Billard, J. Doussot, E. Hertz, B. Lavorel, and O. Faucher
Laboratoire Interdisciplinaire Carnot de Bourgogne, UMR 6303 CNRS-Université Bourgogne Franche-Comté, 9 Av. A. Savary, BP 47870, F-21078 Dijon Cedex, France

(Received 17 June 2015; revised manuscript received 18 September 2015; published 12 November 2015)

Manipulating at will the propagation dynamics of high power laser pulses is a long-standing dream whose accomplishment would lead to the control of fascinating physical phenomena emerging from laser-matter interaction. The present work represents a significant step towards such a control by manipulating the nonlinear optical response of the gas medium. This is accomplished by shaping an intense laser pulse experiencing filamentation at the subcycle level with a relatively weak ($\simeq$1%) third-harmonic radiation. The control results from quantum interference between a single- and a two-color (mixing the fundamental frequency with its third-harmonic) ionization channel. This mechanism, which depends on the relative phase between the two electric fields, is responsible for wide refractive index modifications in relation with significant enhancement or suppression of the ionization rate. As a first application, we demonstrate the production and control of an axially modulated plasma channel.

DOI: 10.1103/PhysRevA.92.053417 PACS number(s): 32.80.Qk, 32.80.Wr, 42.65.Jx, 42.65.Hw

I. INTRODUCTION

When an ultrashort and ultraintense pulse propagates in a transparent medium, the beam is trapped into a self-confined filament capable of sustaining a very high intensity over many linear diffraction lengths along the propagation axis. Since its very first observation in gases [1], much emphasis has been placed on this phenomenon because of its physical interest [2–5], as well as its important applications including terahertz [6] and supercontinuum [7] generation, remote sensing [8], attosecond [9] and high-harmonics [10] physics, spectroscopy [11], machining [12], and lightning protection [13]. Controlling the natural characteristics of a filament and its by-products (such as, for example, the plasma channel left in its wake) by means of a single control parameter would make the filamentation process an even more versatile tool for applications. First attempts devoted to control the filament propagation were realized by using a temporal [14] or a spatial [15–17] pulse shaper eventually coupled with a closed-loop algorithm. Such methods, based on the shaping of the pulse envelope, successfully controlled either the spectral broadening or the plasma channel position. Another way to control the filamentation process based on molecular alignment was also reported [18,19]. By manipulating the rotational degree of freedom of molecules with a strong laser pulse, it was shown that the filament length, continuity, and electron density could be manipulated. More recently, it was reported that an energetic Bessel beam co-propagating with a filament can extend by an order of magnitude the length of the latter [20] by continuously refueling it all along its propagation.

Based on a previous proposal [21], the current work demonstrates that the properties of a filament generated in a gas can be manipulated by controlling the nonlinear optical response of the medium at the microscopic level. The underlying idea relies on a subcycle engineering technique originally used for subfemtosecond spectroscopy [22] and for high-harmonic generation [23]. By seeding the filament with a phase-controlled weak third-harmonic pulse, one can alter the ionization yield and the refractive index so as to modify the attributes of the filament. The technique is first implemented in order to control the length of the filament and its generated supercontinuum. Then, we apply this concept to generate an axially modulated plasma channel. Besides manifesting the control of the nonlinear propagation from microscopic to macroscopic extent by means of a single control parameter, this work also underlines the limitations of the ionization rates used so far in the description of the filamentation process.

II. MANIPULATION OF THE OPTICAL RESPONSE BY HARMONIC SEEDING

In a preliminary experiment, we investigate up to what extent the engineering of an intense infrared (IR) pulse with a weak ultraviolet third-harmonic (TH) beam can modify the optical response of a gas. The experimental setup is provided in Fig. 1(a). Briefly, the optical source is a 1-kHz amplified femtosecond laser delivering horizontally polarized, 3-mJ, 100-fs pulses at $\lambda_0 = 796$ nm. The refractive index change induced by the IR pump beam in a static cell filled with argon at 0.5 bar is measured by the pump-probe cross-defocusing technique [24,25]. In this technique [Fig. 1(a)], a strong pump beam modifies the propagation of the weak probe beam by inducing a spatial and temporal modification to the local refractive index. During the experiment, the two pulses intersect with an angle of about 4° in the horizontal plane inside the cell. Both beams are vertically polarized and focused in the cell with a $f = 15$ cm off-axis parabolic aluminium mirror. After the cell, a coronagraph is inserted in the probe beam path, obstructing it when the pump beam is switched off. It is composed of a fused silica plate at the center of which a 8-mm diameter beam stop has been inserted. On the contrary, if the pump beam induces a local refractive index modification Δn, the probe beam size increases in the far field so that a small amount can propagate around the coronagraph. In the case where the two pulses intersect in the horizontal plane, the cross-defocusing signal lies in the vertical plane as

*pierre.bejot@u-bourgogne.fr

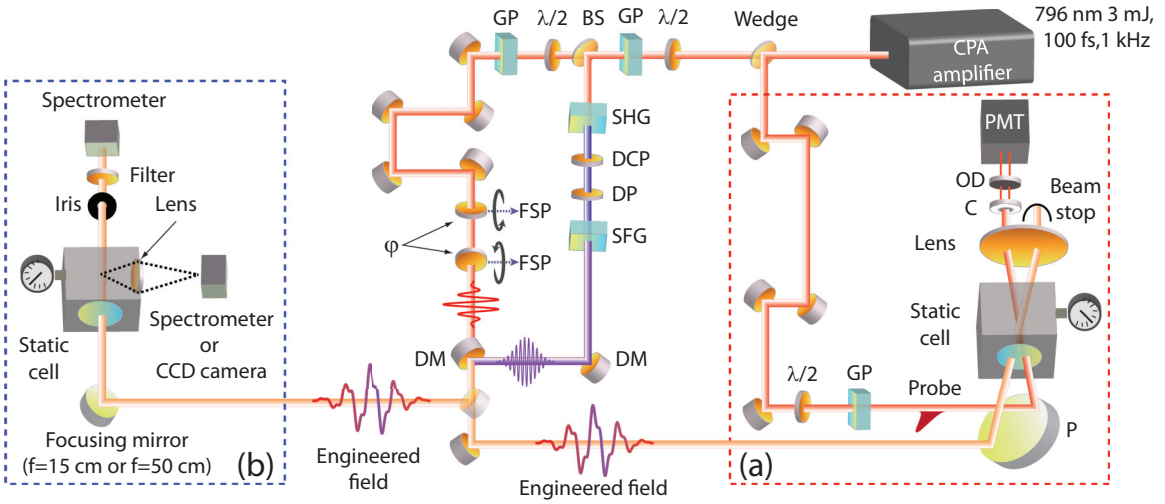

FIG. 1. (Color online) Experimental realization of the electric field engineering. Setup for laser-induced cross-defocusing measurements (a) and for the coherent manipulation of a filament produced in argon (b). BS, beam splitter; GP, glan polarizer; FSP, fused silica plate; OD, neutral optical density; PMT, photomultiplier tube; DM, dichroic mirror; C, coronagraph; DCP, delay compensation plate; DP, dual plate ($\lambda/2$ @796 nm, λ @398 nm); P, parabolic mirror; SHG, second-harmonic generation; SFG, sum-frequency generation.

shown experimentally in Figs. 2(a) and 2(b). The remaining part of the probe propagating around the coronagraph is then redirected to a photomultiplier tube. In the present experiment, the pump-probe delay is about $\tau = 1$ ps. In this case, the cross-defocusing signal only depends on the refractive index change resulting from the ionization mechanism. In order to evaluate this dependence, numerical simulations have been performed. In the Drude model approximation, the nonlinear refractive index Δn induced by the presence of a plasma with electron density ρ is

$$\Delta n = -\frac{\rho}{2\rho_c}, \tag{1}$$

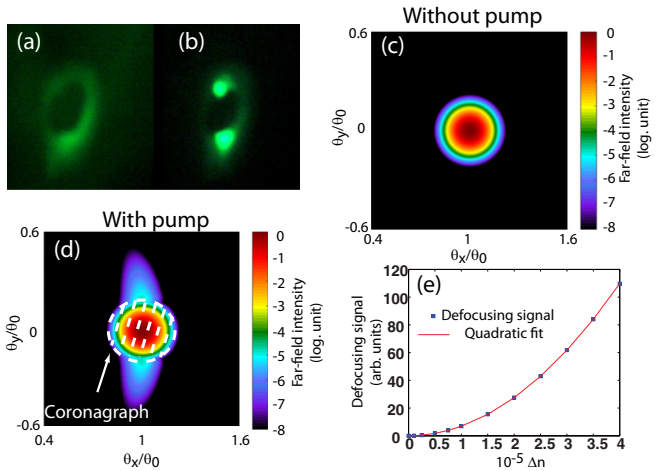

FIG. 2. (Color online) Cross-defocusing technique. Experimental far-field intensity of the probe beam after the coronagraph without (a) and with (b) the pump beam. Numerical far-field distribution of the probe beam without (c) and with (d) the pump beam. (e) Numerical cross-defocusing signal (blue squares) as a function of the peak to valley nonlinear refractive index induced by the pump. The red solid line is a quadratic fit of the numerical defocusing signal.

where $\rho_c = \epsilon_0 m_e \omega_0^2/q_e^2$ is the critical plasma density, ϵ_0 is the vacuum permittivity, ω_0 is probe pulse central pulsation, and m_e (q_e) is the electron mass (charge). The simulation of the cross-defocusing technique has been performed by solving the coupled 2D + 1 equations driving the propagation of both pump $\varepsilon_{\text{pump}}(x,y)$ and probe $\varepsilon_{\text{probe}}(x,y)$ pulses. In a first approximation, they read

$$\partial_z \widetilde{\varepsilon}_{\text{pump}} = i\sqrt{k_0^2 - k_x^2 - k_y^2}\,\widetilde{\varepsilon}_{\text{pump}}, \tag{2}$$

$$\partial_z \widetilde{\varepsilon}_{\text{probe}} = i\sqrt{k_0^2 - k_x^2 - k_y^2}\,\widetilde{\varepsilon}_{\text{probe}} + ik_0\widetilde{\Delta n}\varepsilon_{\text{probe}}, \tag{3}$$

with k_0 the pump and probe wave vector modulus, k_x and k_y are the variables of the reciprocal space associated with x and y, and where $\tilde{A}(k_x,k_y)$ denotes the two-dimensional Fourier transform of a function $A(x,y)$. The refractive index change Δn induced by the pump has been evaluated as

$$\Delta n(x,y) = \Delta n_0 \frac{|\varepsilon_{\text{pump}}|^{2K}(x,y)}{I_0^K}, \tag{4}$$

where $K = 7.5$ is the nonlinearity of the plasma generation in argon for 800-nm pulses [26] and Δn_0 is the refractive index change corresponding to the peak intensity I_0. The initial pump and probe electric fields were defined as

$$\varepsilon_{\text{pump}}(x,y,z=z_0) = \varepsilon_0 e^{\frac{(x-x_0)^2+y^2}{\sigma^2}} e^{-ik_0 \sin\theta x}, \tag{5}$$

$$\varepsilon_{\text{probe}}(x,y,z=z_0) = \varepsilon_1 e^{\frac{(x+x_0)^2+y^2}{\sigma^2}} e^{ik_0 \sin\theta x}, \tag{6}$$

where $\theta = 2^\circ$, $x_0 = -z_0 \tan\theta$, $\sigma = 100\,\mu$m, and $z_0 = -2$ cm. Figures 2(c) and 2(d) display the far field distribution of $\varepsilon_{\text{probe}}$, with and without the pump, evaluated at $z = 2$ cm, i.e., after the pump-probe interaction and confirm that the cross-defocusing signal lies in the vertical plane. As shown in Fig. 2(e), the defocusing signal recorded by the photomultiplier tube is proportional to Δn^2 and accordingly proportional to the square

of the amount of free electrons generated by the pump. It then allows for a direct experimental measurement of the latter.

The subcycle engineering of the pump electric field is realized by superimposing spatially and temporally to the pump a weak TH beam with central wavelength $\lambda_{TH} = \lambda_0/3$. The third-harmonic beam is produced in a commercial module by sum frequency generation in a BBO crystal between the fundamental pulse and its second harmonic, the latter being previously produced in another BBO crystal. As shown in Fig. 1, the relative phase between the two electric fields is controlled by inserting into the pump optical path two identical fused silica plates that rotate symmetrically with respect to a plane perpendicular to the propagation direction. Rotating the two plates then slightly modulates the optical path length and accordingly the relative phase φ between the two pulses, leaving the beam pointing direction unchanged. In order to calibrate experimentally the dephasing induced by rotating the plates, we inserted them into an HeNe laser-based Michelson interferometer. The interference pattern was then analyzed as a function of the rotation of the plates which provided a direct calibration of the phase control setup. The temporal sampling, limited by the minimal step of the motor used to rotate the plates, was about 30 points per third-harmonic optical cycle, which corresponds to a 30-as resolution in the relative delay between the IR and TH pulses.

The experimental results are shown in Figs. 3(a)–3(d). Shaping the pump electric field with a weak TH beam with a central wavelength $\lambda_{TH} = \lambda_0/3$ strongly impacts the ionization yield. The red (respectively, blue) curves depict the ionization as a function of the TH beam energy when the two electric fields are in phase (respectively, out-of-phase).

Our measurements are compared with the numerical simulations obtained by solving the three-dimensional time-dependent Schrödinger equation (TDSE) capturing the quantum dynamics of argon in the single active electron approximation [27]. Within the dipole approximation, the three-dimensional TDSE describing the evolution of the electron wave function $|\psi\rangle$ in the presence of an electric field $\mathbf{E}(t)$ reads

$$i\frac{d|\psi\rangle}{dt} = (H_0 + H_{\rm int})|\psi\rangle, \tag{7}$$

where $H_0 = \nabla^2/2 + V_{\rm eff}$ is the atom Hamiltonian, $H_{\rm int} = \mathbf{A}(t)\cdot\boldsymbol{\pi}$, where $\mathbf{A}(t)$ is the vector potential such that $\mathbf{E}(t) = -\partial\mathbf{A}/\partial t$ and $\boldsymbol{\pi} = -i\nabla$ is the interaction term expressed in the velocity gauge. The effective potential $V_{\rm eff}$ of argon used in the calculation accurately fits the argon eigenenergies and wave functions [28]. The time-dependent wave function $|\psi\rangle$ is expanded on a finite basis of B splines allowing memory efficient fast numerical calculations with a very large basis set [29]:

$$\psi(\mathbf{r},t) = \sum_{l=0}^{l_{\rm max}}\sum_{i=1}^{n_{\rm max}} c_i^l(t)\frac{B_i^k(r)}{r}Y_l^0(\theta,\phi), \tag{8}$$

where B_i^k and Y_l^m are B-spline functions and spherical harmonics, respectively. The basis parameters ($l_{\rm max}$, $n_{\rm max}$, k, and the spatial box size) and the propagation parameters are chosen to ensure convergence. The atom is initially in the ground state (3p) and the electric field E is linearly polarized along

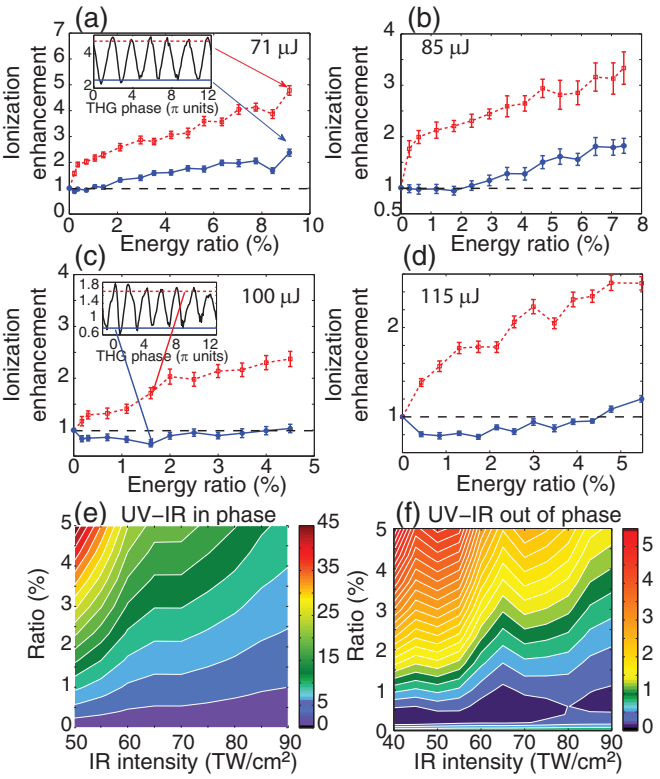

FIG. 3. (Color online) Modification of the nonlinear optical properties of argon by the electric field engineering technique. (a)–(d) Ionization yields as a function of the TH energy (expressed in % of the energy of the IR pulse) for different IR energies $E_{\rm IR}$ (a) 71 μJ, (b) 85 μJ, (c) 100 μJ, and (d) 115 μJ. The peak intensities $I_{\rm IR}$ (expressed in TW/cm^2) can be approximated by $I_{\rm IR} \simeq 0.5E_{\rm IR}$, where $E_{\rm IR}$ is expressed in μJ. The dash red (solid blue) curves correspond to the relative phase maximizing (minimizing) the ionization yield. The error bars correspond to one standard deviation of the ionization yield modification measured at a given phase. The insets show the experimental ionization yield modification as a function of the relative phase between the two electric fields. (e) and (f) Calculated ionization enhancement as a function of both IR and TH intensities for constructive (e) and destructive (f) interferences. The calculations have been performed with a 20-cycle laser pulse in order to reduce the computation time.

the z axis and is expressed as $E(t) = E_0\cos^2(t/\sigma_t)\sin(\omega_0 t)$ for $|t| < \pi N/\omega_0$, where ω_0 is the central frequency of the laser, $\sigma_t = 2N/\omega_0$, and N the total number of optical cycles within the pulse. The simulations are performed for a laser wavelength of 800 nm and a pulse duration corresponding to $N = 20$ cycles. The third-harmonic electric field is expressed as $E_{\rm TH}(t) = \sqrt{R}E_0\cos^6[t/\sigma_t]\sin[3\omega_0 t + \theta]$, where θ is linked with the relative phase between fundamental and third-harmonic electric fields φ by $\varphi = \pi - \theta$ and R is the relative intensity of the third harmonic with respect to the fundamental. The calculated ionization enhancement evaluated as a function of both IR and TH peak intensities is shown in Figs. 3(e) and 3(f) for $\varphi = 0$ (in-phase) and $\varphi = \pi$ (out-of-phase), respectively. Despite a slight overestimation of the ionization enhancement, the numerical results well reproduce the basic features observed experimentally.

The phase dependence of the ionization yield, displayed in the insets of Figs. 3(a) and 3(c), can be interpreted as quantum interferences between different ionization pathways [21]. In this picture, the quantum channel involving only IR pump photons interferes with a channel mixing IR and a single-TH photon. Interference occurs because the two ionization channels connect the same initial and final states. As a consequence, the ionization depends on the relative phase between the two electric fields, the enhancement (respectively, decrease) corresponding to constructive (respectively, destructive) quantum interferences. Alternatively, our result can be explained as well by looking at the total electric field shape applied to the system. In the "electric field" picture, the enhancement of the ionization takes place for the relative phase maximizing the peak of the total field, i.e., when the positive (respectively, negative) peaks of the IR field match with a positive (respectively, negative) peak of the TH field. As a result, since ionization depends, in this regime, on the peak electric field, it also depends on the relative phase. The two descriptions can also be used in the case of two incommensurable frequencies, i.e., when the central frequency of the weak control field does not correspond anymore to the third harmonic of the IR beam. By solving the full TDSE, we recently showed [21] that ionization does not depend anymore on the relative phase between the two fields, even though there is a two-color ionization channel. In the "quantum interferences" picture, the single- and two-color channels do not reach the same final state and therefore cannot interfere. As a result, the ionization is phase independent. It can be understood as well in the "electric field" picture since the peaks of the fundamental field are not synchronized with those of the control field all along the interaction, whatever the introduced relative phase. The two descriptions then seem to be equivalent. There are, however, situations where the "electric field" picture fails at describing the ionization process. This is, for instance, the case of the pure multiphoton regime, where it has been shown that the maximal ionization does not occur when the total field is maximum [30]. In that case, the suited approach for describing the modulation is the one based on interference channels.

III. CONTROL OF THE FILAMENTATION PROCESS BY HARMONIC SEEDING

The ability to manipulate the nonlinear optical response of a medium by a simple shaping of the carrier electric field opens new possibilities for controlling the propagation dynamics of intense laser pulses and, consequently, the underlying applications deriving from it. In order to explore such a possibility, we performed an experiment, in which the carrier electric field of a 1-mJ 100-fs pulse undergoing filamentation is engineered by a 30-μJ TH pulse. The corresponding setup is shown in Fig. 1(b). When recording the output spectrum of the filament that has experienced a strong broadening due to nonlinear propagation, the spectral region lying between 750 and 850 nm is filtered out with a bandpass filter in order to avoid the saturation of the spectrometer. At the same time, the fluorescence of the plasma channel left in the wake of the filament is imaged by the side of the cell on a charge-coupled device camera. In order to confirm that the signal collected by the camera was only due to fluorescence and not to laser scattering, a spectrometer was first put in place of the camera. The camera and the two spectrometers were synchronously triggered with the stepper motor used to rotate the two fused silica plates, allowing one to record the laser spectrum, the plasma channel, and the gas fluorescence spectrum as a function of the relative phase between the two electric fields.

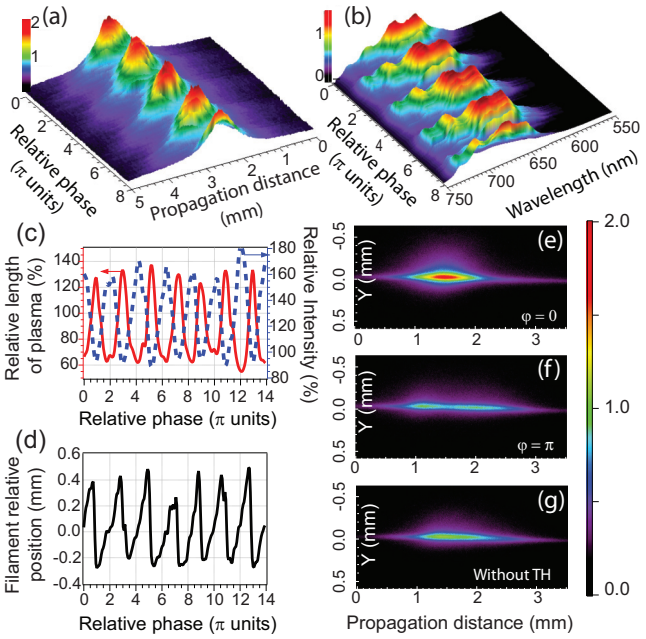

FIG. 4. (Color online) Control of a filament by subcycle engineering in the tightly focused regime. (a)–(d) Modification of the filament properties as a function of φ. (a) Longitudinal profile of the plasma column. (b) Supercontinuum generation. (c) Plasma column length (solid red) and fluorescence (dashed blue). (d) Filament position. (e)–(g) Image of the filament for constructive (e) and destructive (f) quantum interferences between the different ionization channels compared to the case where the filament propagates without the control TH field (g).

Figure 4(a) [respectively, Fig. 4(b)] displays the longitudinal profile of the generated plasma channel (respectively, the supercontinuum) as a function of the relative phase φ between the two electric fields obtained in the tight focusing geometry ($f = 15$ cm) in argon at 1.5-bar pressure. In this case, φ remains almost constant over the 2-mm-long filament because the dephasing induced by the phase velocity mismatch is negligible. As shown in Fig. 4, the engineered filament and the plasma left in its wake experience a strong reshaping depending on the φ value. In particular, in-phase fields favor the production of a short and bright filament [Figs. 4(a) and 4(c)], shifting its position towards the focusing mirror [Fig. 4(d)] and broadening the generated supercontinuum [Fig. 4(b)]. Changing the phase of the TH field then amounts to modulating the ionization rate that the IR field would experience as if it were alone. The plasma fluorescence for the two extremal cases that correspond to constructive ($\varphi = 0$) and destructive ($\varphi = \pi$) quantum interferences are shown in Figs. 4(e) and 4(f). This two cases can be compared to the one

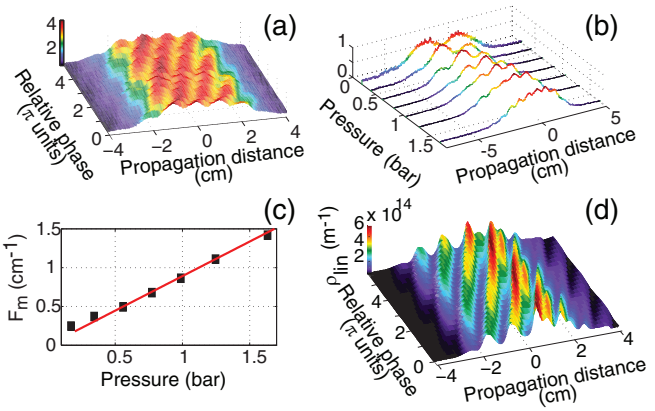

FIG. 5. (Color online) Production and control of an axially modulated plasma channel in the loose focusing regime. Experimental plasma fluorescence (a) along the propagation axis as a function of φ for a pressure of 1 bar. (b) Experimental modulated plasma channel as a function of the pressure. (c) Experimental (black squares) and theoretical [red solid line, calculated as $(n_{\lambda_{\rm TH}} - n_{\lambda_0})/\lambda_{\rm TH}$, where n_λ is the refractive index] modulation frequency $F_{\rm m}$ of the plasma channel as a function of the pressure. (d) Theoretical linear plasma density $\rho_{\rm lin}$ along the propagation axis as a function of φ for a pressure of 1 bar.

in which the filamentation occurs without the control TH field [Fig. 4(g)].

Next, we consider a filament generated in loose focusing geometry ($f = 50$ cm). In this case, φ does not remain constant over the 6-cm-long filament. The two electric fields experience several periodic rephasing/dephasing cycles, with the period being determined by the difference between their respective phase velocities. More particularly, one can define the rephasing length $l_{\rm reph}$ as

$$l_{\rm reph} = \lambda_{\rm TH}\left(\frac{1}{n_{\lambda_{\rm TH}} - n_{\lambda_0}}\right), \tag{9}$$

where n_{λ_0} (respectively, $n_{\lambda_{\rm TH}}$) is the refractive index of the gas at the IR (respectively, TH) laser central wavelength. After a propagation over a distance $l_{\rm reph}$, φ increases by 2π. For a pressure of 1 bar, $l_{\rm reph} \simeq 1$ cm. As a consequence, the plasma channel is axially modulated with a modulation period of $l_{\rm reph} \simeq 1$ cm. By tuning the initial relative phase between the two electric fields, the plasma channel extrema positions continuously shift along the propagation distance as shown in Fig. 5(a). As depicted in Fig. 5(b), the period can be controlled by adjusting the pressure, i.e., by changing the phase velocity mismatch between the two electric fields. The resulting modulation frequency $F_{\rm m} = 1/l_{\rm reph}$ follows the expected linear pressure dependence depicted in Fig. 5(c). Note that the periodicity of the plasma channel could also be controlled at a given pressure by using Bessel beams since the phase velocity of such beams depends on their cone angles [31,32].

Simulating laser pulse propagation over macroscopic distances in a medium undergoing ionization is complicated by the need to include quantum-mechanical laser-atom dynamics. While ionization yield calculations in atoms are routinely performed by solving the time-dependent Schrödinger equation, its consideration in the context of two-dimensional laser propagation requires prohibitive numerical resources. For this reason, standard filamentation codes approximate the ionization yield using a simplified analytic formula [33] originally developed for purely monochromatic laser fields. More specifically, in the presence of a field and its third harmonic, the ionization rate $W(\lambda_0,\lambda_{\rm TH})$ has been evaluated so far [35–39] as

$$W(\lambda_0,\lambda_{\rm TH}) = W[I_0(t)] + W[I_{\rm THG}(t)], \tag{10}$$

where I_0 ($I_{\rm THG}$) is the fundamental (third-harmonic) intensity and W is a monochromatic ionization rate. This phase independent equation implicitly assumes that ionization channels mixing IR and TH fields are negligible as compared to the monochromatic channels, in contradiction to our theoretical and experimental observations [21]. To the best of our knowledge, only one pioneer work [40] tackled analytically the problem of ionization induced by a field and its harmonics. However, the analytical formula presented in this work qualitatively disagrees with our TDSE results because of oversimplifications. For instance, the analytical formula does not predict any ionization enhancement when the two fields are in phase quadrature, in contrast with our TDSE calculations and experimental observations. In order to reproduce the experiment presented in Fig. 5(a), a numerical model of two-color ionization describing the ionization rate as a function of the fundamental pulse intensity, the intensity ratio, and the relative phase between the fields has been developed. This numerical model, valid for a 800-nm fundamental pulse interacting with argon atoms, was included in a propagation code based on the unidirectional pulse propagation equation [41]. More particularly, assuming a cylindrical symmetry around the propagation axis z, the evolution along z of an electric field $\mathbf{E}(r,t,z) = E(r,t,z)\mathbf{e_x}$ linearly polarized along a direction $\mathbf{e_x}$ is given in the spatial and temporal frequency domain by [41]

$$\partial_z \tilde{E}(k_\perp,\omega,z) = ik_z \tilde{E}(k_\perp,\omega,z) + \frac{\mu_0}{2k_z}(i\omega^2 \tilde{P}_{\rm NL} - \omega \tilde{J}), \tag{11}$$

where μ_0 is vacuum magnetic permeability, c is the light velocity in vacuum, $k_z \doteq \sqrt{n^2(\omega)\omega^2/c^2 - k_\perp^2}$ with $n(\omega)$ the frequency-dependent refractive index, and $k_\perp$ the transverse component of the wave vector, and $\tilde{A}$ denotes the Fourier Hankel transform of A:

$$\tilde{A}(k_\perp,\omega) = \int_0^\infty \int_{-\infty}^\infty r A(r,t) J_0(k_\perp r) e^{i\omega t} dt dr, \tag{12}$$

with J_0 the zeroth-order Bessel function. The nonlinear polarization $P_{\rm NL}$ and the free charges induced current J are evaluated as

$$\begin{aligned} P_{\rm NL}(r,t) &= \epsilon_0 \chi^{(3)} E^3(r,t), \\ \tilde{J}(k_\perp,\omega) &= \frac{q_e^2(\nu_e + i\omega)}{m_e(\nu_e^2 + \omega^2)} \widetilde{\rho E}, \end{aligned} \tag{13}$$

where ν_e is the effective electron-ion collision frequency and $\chi^{(3)}$ is the third-order nonlinear susceptibility. The initial electric field $E(r,t,z=0)$ is composed of a 1-mJ, 100-fs, 800-nm fundamental pulse and a 30-μJ, 70-fs, 266-nm third-harmonic pulse. Both pulses are focused at $f = 50$ cm and

have an initial waist $\sigma_0 = 2$ mm. The free electron density was evaluated in two different ways as

$$\partial_t \rho(r,t) = \rho_{\rm at} G[I_0(r,t), I_{\rm THG}(r,t), \varphi(r)] W_{\omega_0}, \quad (14)$$

or

$$\partial_t \rho(r,t) = \rho_{\rm at}\left(W_{\omega_0} + W_{3\omega_0}\right), \quad (15)$$

where $\rho_{\rm at}$ is the atomic density, W_{ω_0} ($W_{3\omega_0}$) is the PPT ionization rate [33] evaluated at the frequency ω_0 ($3\omega_0$), I_0 ($I_{\rm THG}$) is the fundamental (third-harmonic) intensity, $\varphi = \phi(3\omega_0) - 3\phi(\omega_0)$ with $\phi(\omega_0)$ [respectively, $\phi(3\omega_0)$] the phase of the field evaluated at ω_0 (respectively, $3\omega_0$), and G the ionization rate enhancement induced by the quantum channel interferences. The latter has been evaluated by performing an extensive parametric study of the time-dependent Schrödinger equation as a function of I_0, $I_{\rm THG}$, and φ [34]. During this study, square 50-fs pulses with two cycles turn-on and turn-off were used, allowing one to keep constant all along the interaction the fundamental intensity and also the ratio between the fundamental and third-harmonic intensities. For each fundamental intensity I_0 (from 1 to 100 TW/cm^2 by a step of 0.5 TW/cm^2) and relative phase φ (from 0 to 2π by step of 0.1π), the intensity of the third harmonic has been varied from 0% to 25% by a step of 0.1%. At the end of the interaction, the population promoted in the continuum was recorded allowing one to evaluate the total ionization enhancement $\mathcal{G}$. We finally checked that the ionization rate enhancement G is equal in a good approximation to $\mathcal{G}$ as long as the ionization remains low ($<10^{-2}$). During the propagation calculation, $G(r,t)$ was evaluated with the help of a three-dimensional cubic spline interpolation of the set of data calculated with TDSE.

The longitudinal distribution of the linear plasma density obtained according to our propagation code embedding our numerical phase-dependent two-color ionization rate is shown in Fig. 5(d). It is in fair agreement with the experiment reported in Fig. 5(a). Note that substituting the two-color phase sensitive ionization rate by a standard ionization rate [Eq. (15)] leads to numerical results that are inconsistent with the experimental observations. This underlines the necessity to improve the way ionization is evaluated in propagation codes. In particular, while the present experimental results have been obtained by externally seeding the filament with a third-harmonic beam, it is known that the latter is self-generated at the percent level during the propagation of a filament [35,36]. A rational question arising from the present work is up to what extent the self-induced third-harmonic seeding impacts the propagation dynamics of a filament by the exhibited TH-IR interference effect. This question will be developed in a further study.

IV. CONCLUSION

In summary, we have experimentally and theoretically demonstrated that the nonlinear optical properties of a gas experienced by a strong ultrashort laser pulse can be manipulated by a subcycle engineering of the latter. The control has been realized by adding a realistically weak third-harmonic beam that propagates together with the fundamental, intense laser pulse. Because of quantum interferences occurring during the ionization process, ionization can be either suppressed or enhanced depending on the relative phase between the two electric fields. We have applied this phenomenon to the control of the nonlinear propagation dynamics of a strong laser beam experiencing filamentation. More particularly, we have succeeded in manipulating the macroscopic characteristics of a filament (supercontinuum generation, plasma column length, amplitude, and position) by adjusting the relative phase between the two electric fields. Moreover, taking advantage of the phase velocity mismatch between the two electric fields, we have created and controlled a sinuslike plasma channel. Being based on a nonresonant quantum process, the present mechanism potentially takes place in any gas and even in bulk materials.

ACKNOWLEDGMENTS

This work was supported by the Conseil Régional de Bourgogne (PARI program), the CNRS, the French National Research Agency (ANR) through the CoConicS program (Contract No. ANR-13-BS08-0013) and the Labex ACTION program (Contract No. ANR-11-LABX-0001-01). P.B. thanks the CRI-CCUB for CPU loan on its multiprocessor server. The authors gratefully acknowledge V. Tissot and J.-M. Muller for the cell conception and Professor D. Charalambidis and Professor J.-P. Wolf for discussions.

[1] A. Braun, G. Korn, X. Liu, D. Du, J. Squier, and G. Mourou, Opt. Lett. **20**, 73 (1995).
[2] S. L. Chin, S. A. Hosseini, W. Liu, Q. Luo, F. Theberge, N. Aközbek, A. Becker, V. P. Kandidov, O. G. Kosareva, and H. Schroeder, Can. J. Phys. **83**, 863 (2005).
[3] L. Bergé, S. Skupin, R. Nuter, J. Kasparian, and J.-P. Wolf, Rep. Prog. Phys. **70**, 1633 (2007).
[4] A. Couairon and A. Mysyrowicz, Phys. Rep. **441**, 47 (2007).
[5] J. Kasparian and J.-P. Wolf, Opt. Express **16**, 466 (2008).
[6] C. D'Amico, A. Houard, M. Franco, B. Prade, A. Mysyrowicz, A. Couairon, and V. T. Tikhonchuk, Phys. Rev. Lett. **98**, 235002 (2007).
[7] N. Akozbek, M. Scalora, C. M. Bowden, and S. L. Chin, Opt. Commun. **191**, 353 (2001).
[8] J. Kasparian, M. Rodriguez, G. Méjean, J. Yu, E. Salmon, H. Wille, R. Bourayou, S. Frey, Y.-B. André, A. Mysyrowicz, R. Sauerbrey, J.-P. Wolf, and L. Wöste, Science **301**, 61 (2003).
[9] A. Couairon, H. S. Chakraborty, and M. B. Gaarde, Phys. Rev. A **77**, 053814 (2008).
[10] D. S. Steingrube, E. Schulz, T. Binhammer, M. B. Gaarde, A. Couairon, U. Morgner, and M. Kovačev, New J. Phys. **13**, 043022 (2011).
[11] K. Stelmaszczyk, P. Rohwetter, G. Méjean, J. Yu, E. Salmon, J. Kasparian, R. Ackermann, J.-P. Wolf, and L. Wöste, Appl. Phys. Lett. **85**, 3977 (2004).

[12] D. Kiselev, L. Woeste, and J.-P. Wolf, Appl. Phys. B **100**, 515 (2010).
[13] J. Kasparian, R. Ackermann, Y.-B. André, G. Méchain, G. Méjean, B. Prade, P. Rohwetter, E. Salmon, K. Stelmaszczyk, J. Yu, A. Mysyrowicz, R. Sauerbrey, L. Wöste, and J.-P. Wolf, Opt. Express **16**, 5757 (2008).
[14] R. Ackermann, E. Salmon, N. Lascoux, J. Kasparian, P. Rohwetter, K. Stelmaszczyk, S. Li, A. Lindinger, L. Wöste, P. Béjot, L. Bonacina, and J.-P. Wolf, Appl. Phys. Lett. **89**, 171117 (2006).
[15] G. Heck, J. Sloss, and R. J. Levis, Opt. Commun. **259**, 216 (2006).
[16] T. Pfeifer, L. Gallmann, M. J. Abel, D. M. Neumark, and S. R. Leone, Opt. Lett. **31**, 2326 (2006).
[17] D. Walter, S. Eyring, J. Lohbreier, R. Spitzenpfeil, and C. Spielmann, Appl. Phys. B **88**, 175 (2007).
[18] S. Varma, Y.-H. Chen, and H. M. Milchberg, Phys. Rev. Lett. **101**, 205001 (2008).
[19] S. Varma, Y.-H. Chen, J. P. Palastro, A. B. Fallahkair, E. W. Rosenthal, T. Antonsen, and H. M. Milchberg, Phys. Rev. A **86**, 023850 (2012).
[20] M. Scheller, M. S. Mills, M.-A. Miri, W. Cheng, J. V. Moloney, M. Kolesik, P. Polynkin, and D. N. Christodoulides, Nat. Photon. **8**, 297 (2014).
[21] P. Béjot, G. Karras, F. Billard, E. Hertz, B. Lavorel, E. Cormier, and O. Faucher, Phys. Rev. Lett. **112**, 203902 (2014).
[22] A. Wirth, M. Th. Hassan, I. Grguraš, J. Gagnon, A. Moulet, T. T. Luu, S. Pabst, R. Santra, Z. A. Alahmed, A. M. Azzeer, V. S. Yakovlev, V. Pervak, F. Krausz, and E. Goulielmakis, Science **334**, 195 (2011).
[23] S. Haessler, T. Balčiunas, G. Fan, G. Andriukaitis, A. Pugžlys, A. Baltuška, T. Witting, R. Squibb, A. Zaïr, J. W. G. Tisch, J. P. Marangos, and L. E. Chipperfield, Phys. Rev. X **4**, 021028 (2014).
[24] V. Renard, O. Faucher, and B. Lavorel, Opt. Lett. **30**, 70 (2005).
[25] V. Loriot, E. Hertz, A. Rouzee, B. Sinardet, B. Lavorel, and O. Faucher, Opt. Lett. **31**, 2897 (2006).
[26] F. Billard, P. Béjot, E. Hertz, B. Lavorel, and O. Faucher, Phys. Rev. A **88**, 013854 (2013).
[27] P. Béjot, E. Cormier, E. Hertz, B. Lavorel, J. Kasparian, J.-P. Wolf, and O. Faucher, Phys. Rev. Lett. **110**, 043902 (2013).
[28] H. G. Muller, Phys. Rev. A **60**, 1341 (1999).
[29] H. Bachau, E. Cormier, P. Decleva, J. E. Hansen, and F. Martin, Rep. Prog. Phys. **64**, 1815 (2001).
[30] K. J. Schafer and K. C. Kulander, Phys. Rev. A **45**, 8026 (1992).
[31] D. Mugnai, A. Ranfagni, and R. Ruggeri, Phys. Rev. Lett. **84**, 4830 (2000).
[32] B. D. Layer, A. York, T. M. Antonsen, S. Varma, Y.-H. Chen, Y. Leng, and H. M. Milchberg, Phys. Rev. Lett. **99**, 035001 (2007).
[33] A. M. Perelomov, V. S. Popov, and M. V. Terentev, Sov. Phys. JETP **23**, 924 (1966).
[34] J. Doussot, P. Béjot, G. Karras, F. Billard, and O. Faucher, J. Phys. B **48**, 184005 (2015).
[35] L. Bergé, S. Skupin, G. Méjean, J. Kasparian, J. Yu, S. Frey, E. Salmon, and J.-P. Wolf, Phys. Rev. E **71**, 016602 (2005).
[36] N. Aközbek, A. Iwasaki, A. Becker, M. Scalora, S. L. Chin, and C. M. Bowden, Phys. Rev. Lett. **89**, 143901 (2002).
[37] Y. Liu, M. Durand, A. Houard, B. Forestier, A. Couairon, and A. Mysyrowicz, Opt. Commun. **284**, 4706 (2011).
[38] M. B. Gaarde and A. Couairon, Phys. Rev. Lett. **103**, 043901 (2009).
[39] M. Kolesik, E. M. Wright, and J. V. Moloney, Opt. Lett. **32**, 2816 (2007).
[40] A. M. Perelomov and V. S. Popov, Sov. Phys. JETP **25**, 336 (1967).
[41] M. Kolesik and J. V. Moloney, Phys. Rev. E **70**, 036604 (2004).